John L. Volakis
ElectroScience Lab
Elecrical Engineering Dept.
The Ohio State University
1320 Kinnear Rd.
Columbus, OH 43212
+1 (614) 292-5846 Tel.
+1 (614) 292-7297 (Fax)
volakis.1@osu.edu (email)

David B. Davidson
Dept. E&E Engineering
University of Stellencosch
Stellenbosch 7600, South Africa
(+27) 21 808 4458
(+27) 21 808 4981 (Fax)
davidson@ing.sun.ac.za (e-mail)

Foreword by the Editors

Properly terminating FDTD (Finite-Difference Time-Domain) meshes is without doubt one of the central challenges of the method. As the authors of this month's contribution comment, it is frequently the single most important factor in obtaining reliable results with the FDTD. The PML (perfectly matched layer) concept introduced by Berenger in 1994 revolutionized mesh termination, and is currently the method of first choice. However, as those of us who have implemented the scheme will be aware, its implementation is not entirely trivial, and it does bring some computational overhead with it. In this month's contribution, a new *re-radiating boundary condition* (rRBC) is introduced: it represents a return to some of the original ideas in mesh termination, in that it concentrates on field *cancellation*, rather than *absorption*. An attractive feature of the method is that it offers "dialable" performance, which is obtained by stacking several layers of rRBCs. We thank the authors for this very interesting contribution, which we anticipate will be especially useful to the CEM community. Finally, we would also like to offer the authors our apologies for a slight delay in publishing their paper, occasioned by e-mail problems.

A Simple Stackable Re-Radiating Boundary Condition (rRBC) for FDTD

R. E. Díaz and I. Scherbatko

Arizona State University
E-mail: rudydiaz@asu.edu

Abstract

The fundamental properties of a new re-radiating boundary condition (rRBC) for terminating the grid in the Finite-Difference Time-Domain (FDTD) method are examined. It is shown that because it is based on the Field Teleportation Principle of [1], this rRBC generates exact negative copies of the outgoing time-domain fields in FDTD, independently of the angle of incidence, polarization, field impedance, or material properties. The effect of the rRBC is to differentiate the outgoing signal and reduce it approximately by a factor of 10 in the time domain. Several rRBC boundaries can be stacked, one after the other, to continually decrease the level of the outgoing signal. Termination of the rRBC stack with a one-cell Huygens' condition further reduces the signal, and minimizes the integration feedback as the faint echoes cross backwards through the rRBCs. It is shown that the net result is a boundary that is more efficient than a PML of similar total thickness (especially at shallow angles of incidence) and is trivial to program, requiring no special treatment for corners or material properties.

Keywords: FDTD methods; electromagnetic scattering; equivalent sources; absorbing boundary conditions

1. Introduction

This work is part of a program for creating a simple FDTD engine for teaching electromagnetics and solving practical engineering problems, while at the same time minimizing the programmer's workload. Termination of the FDTD grid in such a way that outgoing traveling waves are not reflected back into the computational domain is the single most important factor in guaranteeing the correctness of the results obtained. Once that artificial reflection is eliminated, many improvements can be made to the basic FDTD Yee-grid formulation to improve its accuracy and accelerate its performance (e.g. [2]).

Berenger's PML [3] and its derivatives [4] are almost universally accepted today as the grid termination of choice. However, implementing a PML is not a trivial undertaking. The programmer must carefully tailor the PML to the materials intersecting the outer boundary, correctly account for edges and corners, and accept the penalty in computational load incurred by the complex update equations in the multi-layer PML. In this paper, we return to the simple idea of canceling the outward-bound waves as a means of effective termination. This idea, implicit in the original work on one-sided wave equations (e.g. Mur's condition), turns out to be trivial to implement explicitly using Field Teleportation [1].

The approach is to define planar boundaries inside the FDTD domain at which the discrete FDTD version of Schelkunoff's equivalent currents are calculated. These currents are then flipped in sign, and used to radiate an exact negative copy of the field crossing the boundary. The only three requirements for this technique to work are: (a) that the tangential fields on the boundary be stored one time step in the past, (b) that the field be re-radiated one space cell forwards of the boundary where the currents are calculated, and (c) that the material properties of the medium be the same at the cells receiving the field as they were at the cell where they were copied.

In the next section, we start the discussion by revisiting Maxwell's first curl equation briefly, to emphasize the difference between induced (material) currents and impressed (source) currents. In this way, it is demonstrated that to properly create discrete Schelkunoff currents in FDTD, the material properties of the environment must be taken into account. Then, the recipe for Field Teleportation is reviewed, and its implementation as an RBC is detailed. Numerical experiments are then performed to demonstrate the synergy between the components of the RBC and its performance as a function of frequency and angle of incidence.

2. Teleportation of Fields

From the outset, we assume that all materials in the FDTD space are dispersive. We will use the simplest such materials for the rest of this paper, namely those containing dc electric and magnetic conductivity. This choice is appropriate because these materials can serve as surrogates for many real materials over considerable bandwidths. This choice is necessary because a key issue in creating true discrete Schelkunoff currents in FDTD is to account for the material properties of the space. The electric and magnetic conductivity can be absorbed into the relative permittivity and permeability operators, $\bar{\bar{\varepsilon}}(t)$, $\bar{\bar{\mu}}(t)$, by using the integration operator. For instance,

$$\bar{\bar{\varepsilon}}(t) = \varepsilon_r + \int dt \frac{\sigma}{\varepsilon_0}, \tag{1}$$

where the double bar indicates that the permittivity is an operator in the time domain. Equation (1) is the time-domain version of the usual frequency-domain expression $\varepsilon(\omega) = \varepsilon_r + \sigma/(j\omega\varepsilon_0)$. We can then define the totally divergenceless displacement vector,

$$\vec{\mathbf{D}}(t) = \bar{\bar{\varepsilon}}(t)\vec{E}(t), \tag{2}$$

such that Maxwell's first curl equation becomes

$$\nabla \times \vec{H} = \frac{\partial \vec{\mathbf{D}}}{\partial t}. \tag{3}$$

In this way, the conventional electric conduction current is absorbed into the total induced current (the right-hand side of Equation (3)). The more familiar form of the right-hand side of Equation (3) can be recovered in the case of a time-invariant conductivity:

$$\frac{\partial \vec{\mathbf{D}}}{\partial t} = \frac{\partial\left[\bar{\bar{\varepsilon}}(t)\varepsilon_0\vec{E}\right]}{\partial t} = \frac{\partial\left(\varepsilon_r\varepsilon_0\vec{E}\right)}{\partial t} + \sigma\vec{E} = \frac{\partial \vec{D}}{\partial t} + \vec{J}_e. \tag{4}$$

The above considerations are necessary to emphasize that all currents induced in a material are taken into account by the dispersive constitutive operators. Since FDTD solves Maxwell's equations by time integration of the total induced current, Maxwell's curl equations in the presence of impressed currents must be written as

$$\begin{aligned} \frac{\partial \vec{\mathbf{D}}}{\partial t} &= \nabla \times \vec{H} - \vec{J}_e, \\ \frac{\partial \vec{\mathbf{B}}}{\partial t} &= -\nabla \times \vec{E} - \vec{J}_m, \end{aligned} \tag{5}$$

where $\vec{J}_{m,e}$ are the impressed electric and magnetic currents. When these are turned into update equations for the force fields ($\vec{E}$ and $\vec{H}$) by direct integration, it becomes clear that whatever the material operators do to the curl term, they must also do to the impressed currents:

$$\mathbf{D}^{n+1} = \mathbf{D}^n + dt\left\{\nabla \times \vec{H}\right\} - dt\left\{\vec{J}_e\right\}. \tag{6}$$

For example, in the case of a moderate (not requiring exponential time-stepping) constant conductivity,

$$\begin{aligned} E^{n+1} = E^n &\left[\frac{1 - \frac{\sigma_e dt}{2\varepsilon_r\varepsilon_0}}{1 + \frac{\sigma_e dt}{2\varepsilon_r\varepsilon_0}}\right] + \frac{dt}{\varepsilon_r\varepsilon_0}\left[\frac{1}{1 + \frac{\sigma_e dt}{2\varepsilon_r\varepsilon_0}}\right]\left\{\nabla \times H\right\}^{n+\frac{1}{2}} \\ &- \frac{dt}{\varepsilon_r\varepsilon_0}\left[\frac{1}{1 + \frac{\sigma_e dt}{2\varepsilon_r\varepsilon_0}}\right]\left\{J_e\right\}^{n+\frac{1}{2}} \end{aligned} \tag{7}$$

$$H^{n+\frac{3}{2}} = H^{n+\frac{1}{2}}\left[\frac{1-\frac{\sigma_m dt}{2\mu_r\mu_0}}{1+\frac{\sigma_m dt}{2\mu_r\mu_0}}\right] - \frac{dt}{\mu_r\mu_0}\left[\frac{1}{1+\frac{\sigma_m dt}{2\mu_r\mu_0}}\right]\{\nabla\times E\}^{n+1}$$
$$-\frac{dt}{\mu_r\mu_0}\left[\frac{1}{1+\frac{\sigma_m dt}{2\mu_r\mu_0}}\right]\{J_m\}^{n+1}.$$

In Equations (7), we see that the impressed currents simply create additional impressed E and H fields (call them δE, δH), driven by the impressed currents but moderated by the material properties of the medium.

The Schelkunoff equivalent currents are then impressed currents defined at a Cartesian surface by

$$\vec{K}_e = \vec{J}_e \cdot ds = \hat{n}\times\vec{H},$$
$$\vec{K}_m = \vec{J}_m \cdot ds = -\hat{n}\times\vec{E}, \tag{8}$$

where ds is the grid size in the direction of the normal (that is, dx, dy, or dz).

All that remains to be explained is the actual location of these currents and the impressed fields they produce relative to the fields they replace. This was given in [1], and it is easiest to see in Figure 1. In the figure, we use a two-dimensional Hz FDTD domain for simplicity, and consider copying (teleporting) a field at a given boundary to an identical boundary in another FDTD domain. As the figure shows, all that needs to be done is to add the δE from the electric surface current created by the H field (according to Equation (8)) into the E-field point on the other side of the surface, and to add the δH from the magnetic surface current created by the E field at that surface into the H-field point on the other side of the surface.

To create an RBC using Field Teleportation, all we need to do is flip the signs of the δE and δH.

3. Implementation of the rRBC in FDTD

The idea of the rRBC is to attenuate the outgoing field to such a degree that when it reflects from the grid termination there is negligible interference with the fields of interest in the solution space. Because it is being implemented inside the FDTD computer code, it is subject to the order implicit in the execution of the various loops within the code. The proper way to implement it is according to the following sequence:

Set $t = t + dt$

1. H field Update using present value of E field.
2. Shift stored tangential E fields from bin#1 to bin#2.
3. Store present tangential E fields in bin#1.
4. Inject δH fields using E fields in bin#2.
5. Use present tangential E fields to create the missing H fields at the Huygens termination.

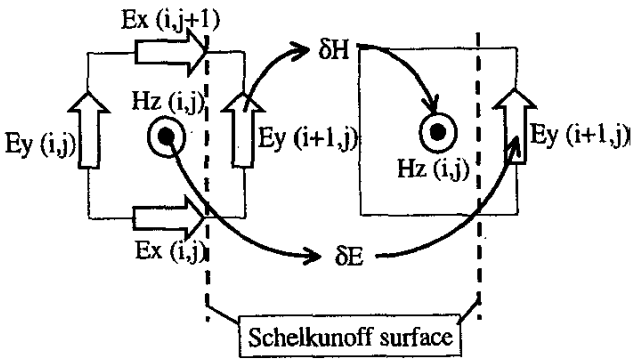

Figure 1. The teleportation recipe for creating an exact copy of an FDTD field in another FDTD space.

6. E field Update using present values of H field.
7. Shift stored tangential H fields from bin#1 to bin#2.
8. Store present tangential H fields in bin#1.
9. Inject δE fields using H fields in bin#2.
10. Use present tangential H fields to create the missing E fields at the Huygens termination.

Return

The Huygens termination is the simplest possible termination for the Yee grid. Consider the two-dimensional FDTD cell in Figure 1, and assume it is one cell of an Nx by Ny space. The matrix for storing the field values is dimensioned from (0 to $Nx+1$, 0 to $Ny+1$) but the update loops are only run from 1 to Nx and 1 to Ny, respectively. If the cell of the figure were the $i = Nx$ cell of the domain, when the H update loop comes up, the Hz field is missing the $\mathrm{Ey}(Nx+1, j)$ information it needs to update itself. Therefore, at the end of the E loop, we create the missing field $\mathrm{Ey}(Nx+1, j)$ not as an update, but simply as $\eta(Nx, j)\mathrm{Hz}(Nx, j)$, where the impedance of the cell is approximated as

$$\eta(i,j) = \sqrt{\frac{\mu(i,j)+\sigma_m(i,j)dt}{\varepsilon(i,j)+\sigma_e(i,j)dt}}. \tag{9}$$

In a three-dimensional Yee grid space, three of the walls require missing H fields to be created, and three require missing E fields to be created (according to the complementary recipe $H_{missing} = E/\eta$). The Huygens termination is equivalent to assuming that the field reaching it is a plane wave at normal incidence. Therefore it is an extremely good termination for normally incident waves, but poor for waves reaching it at shallow angles. However, as we will show in the next section, the rRBC excels at attenuating waves traveling at shallow angles.

Before performing the numerical experiments of the next section, it is appropriate to make a series of observations. First, the simplicity of the rRBC comes with a price: the danger of feedback. If the second cell in Figure 1 exists in the same FDTD domain as the first cell, then it cannot be the same cell, because the teleported fields will feed back into the source fields through the curl operators in the update loops. Therefore, the teleported negative fields

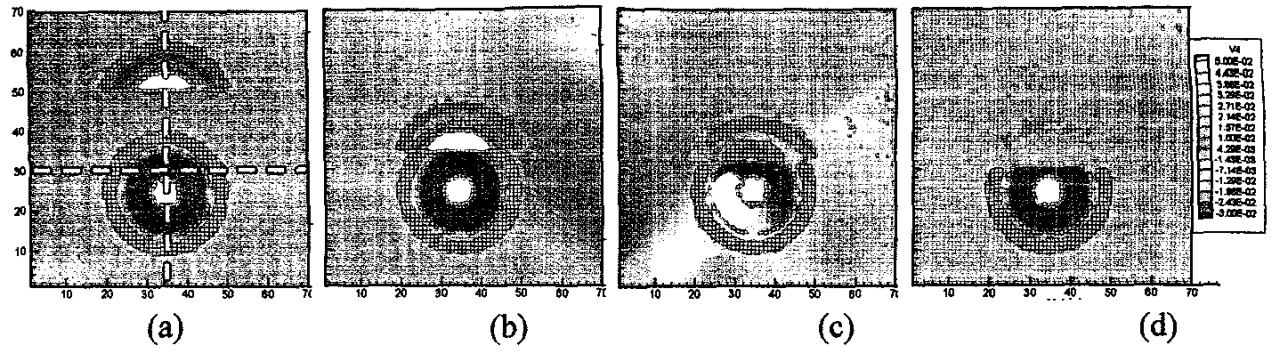

Figure 2. Snapshots of the Ez field on the symmetry plane of a pulsed dipole antenna (seven cells long), with a teleportation boundary four cells in front of the antenna. The field is teleported with a sign reversal 20 cells from the boundary (a), four cells (b), two cells (c), and one cell (d).

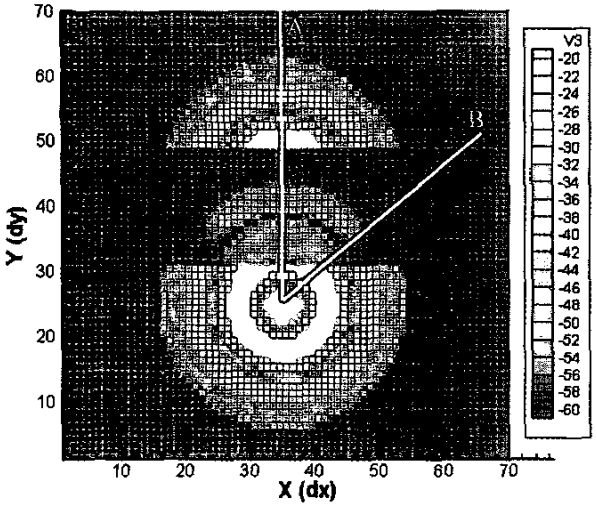

Figure 3a. Simultaneous teleportation 20 cells away with no sign reversal, and one cell away with sign reversal, illustrate the perfect one-sidedness of the teleported field and the strong cancellation of the field upon crossing the subtraction boundary. The color contours have been saturated to magnify the subtracted pulse. Note that the subtracted pulse is more attenuated at angles away from the normal to the surface (B). The worst-case (least) attenuation along line A is approximately –17 dB without distortion.

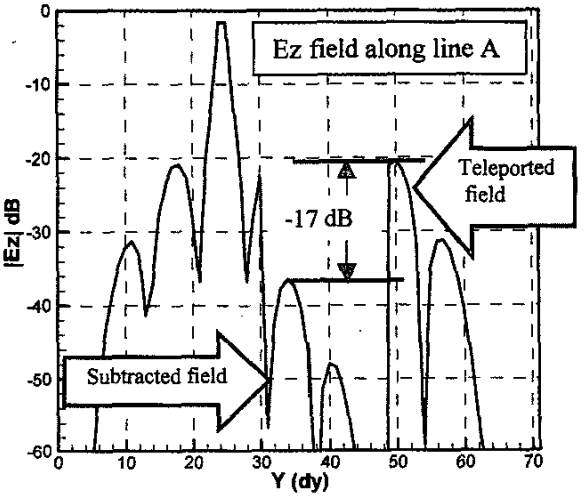

Figure 3b. The Ez field along line A in Figure 3a.

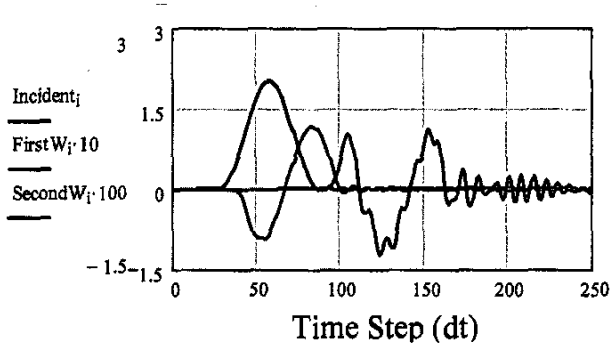

Figure 4a. The time histories of a pulse (black curve) as it crosses one (red curve) and two (blue curve) RBCs. The attenuated pulses have been multiplied by a factor of 10 and 100, respectively, to plot them on the same scale.

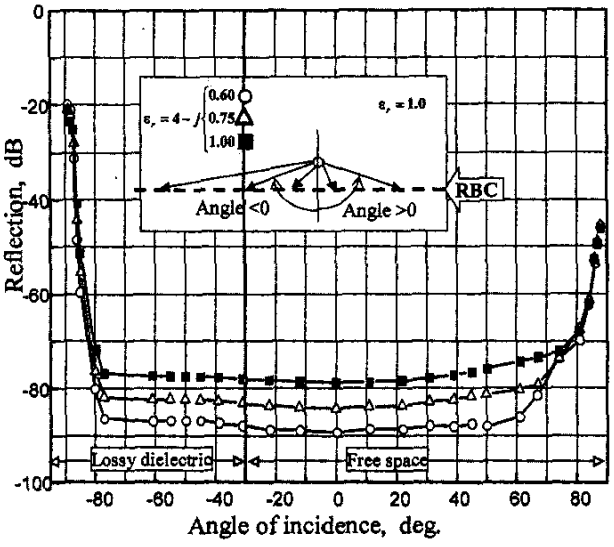

Figure 7. The results from the numerical experiment illustrated in the inset demonstrate the insensitivity of the rRBC's performance to angle of incidence.

must be sent at least one cell beyond the copying boundary. To offset this spatial delay, the programming sequence introduces a one-time-step delay before teleporting (bins#1 and bins#2). Clearly if we had a dispersionless one-dimensional space, this combination of offsets would exactly cancel, and the field subtraction would be perfect. However, the FDTD grid is dispersive, and therefore the FDTD wave does not arrive exactly in phase with the teleported wave, reducing the accuracy of the subtraction. This imperfect subtraction is easily compensated for by stacking rRBCs, placing more of them one after the other. Any subtraction of a time-domain pulse from a slightly shifted copy of itself looks like a dim version of its first derivative, thence the apparent differentiation property of rRBCs that will be seen in the next section.

This leads to the second observation: A pulse encountering the rRBC teleportation boundary from the wrong side would be expected to undergo re-integration but in a strange way, since portions of the pulse that have crossed the boundary find themselves teleported back behind where they first entered the boundary, actually creating excess energy. If we did not have the one-time-step delay buffer in the recipe, this would constitute a fatal flaw in the rRBC. The one-time-step delay reduces this backwards interaction to a mild re-integration of the pulse. It is easy to show that the biggest problem with pulses entering the rRBC boundary from the wrong side is their dc content. Fortunately, on the way forward, the differentiating property of the rRBC strips off most of the dc content of all signals, and so does the Huygens termination. As will be shown, the combination of the rRBC and the Huygens termination is synergistic.

The final observation is that because of the length of the curl stencil in FDTD, it is best to separate successive rRBCs in the stack from each other by two cells (for instance, in a space of 100 cells, at cells $i = 97, 94, 91$, etc.) In principle, in the forward direction they could be spaced only one cell apart, but the problem is that high-frequency noise left in an empty FDTD grid in late time, upon traveling backwards through the RBCs, feeds back on itself. To further reduce this danger poised by numerical-noise feedback, we purposely dampen the copy of the field by the factor 0.99: in other words, we limit the perfect subtraction (which would occur at very low frequencies) to −40 dB per rRBC wall. The combination of the two-cell separation and the 0.99 factor makes the rRBC stack stable against feedback in all experiments we have performed, even extending in the late time to millions of time steps of pure noise. Finally, for time-domain impulse simulations, we routinely use bipolar pulses with zero dc content as our input source.

4. Numerical Experiments

Figure 2 shows a snapshot of the contours of the vertical Ez field on the symmetry plane around a short PEC dipole (seven cells long), excited by a pulse. In Figure 2a, the field that crosses the horizontal dashed line was copied, flipped in sign, and teleported 20 cells away. In Figures 2b, 2c, and 2d, this teleported field was brought progressively closer, until at the prescribed one-cell distance it virtually erased the original field.

Note that the teleportation boundary is only four cells away from the dipole: we are clearly copying and teleporting the near field of the dipole. To emphasize that the teleported field has no backwards radiation (perfect implementation of equivalent currents), we saturated the Ez contours in Figure 3, and show a teleported copy 20 cells away while, at the same time, teleporting a negative copy one cell away. The contours are now in dB. In addition to showing zero backwards radiation from the teleported field, we also note that the faint field left over after subtraction was more attenuated at shallow angles (to the right of line B) than at angles near normal (around line A). The reason for this extra effectiveness is that as the wave's direction of travel approaches the tangent to the boundary, the dispersion error becomes less relevant, and the wave more closely resembles a plane wave.

Since the worst case for dispersion error is near normal incidence, a three-dimensional FDTD space was created to carry a TEM wave along the y axis, guided by PEC and PMC walls. In the first experiment, a unipolar pulse was tracked as it approached and crossed two rRBCs in the forward direction. Figure 4a shows the original pulse (black curve), the pulse after crossing the first rRBC (multiplied by a factor of 10), and the pulse after crossing the second rRBC (multiplied by a factor of 100). Thus, an rRBC typically reduces the peak field of an incident pulse by about −20 dB and differentiates it.

Calculating the spectrum of the original pulse and the two attenuated pulses, we can derive the rRBC attenuation in the frequency domain. This is shown in Figure 4b. The flattening of the performance at −40 dB per wall near dc was the result of our 0.99 factor mentioned above. If this limitation had not been imposed, it is clear that the rRBC attenuation per wall would have been linear at 20 dB per decade per wall.

For the next experiment, we used only one rRBC, and placed a PEC behind it. The incident pulse was a bipolar pulse $55dt$ long, with zero dc content and a peak amplitude of 1.3 V/m. Figure 5a shows the attenuated pulse after crossing the rRBC (solid line), and the resulting re-integrated pulse after the PEC reflection sent it backwards through the rRBC. The pulse returning into the FDTD domain was only −9 dB below the incident pulse. However, if the Huygens termination was behind the rRBC, we get the result of Figure 5b. The solid curve is the pulse after reflecting from the Huygens termination (note the change of scale), and the dashed curve is this pulse after it re-entered into the FDTD domain backwards through the rRBC. The peak of this re-entering pulse was about −37 dB below the original pulse. Thus, for the case of normal incidence, the single rRBC-Huygens termination provided approximately −40 dB attenuation in the time domain.

Comparing the dashed line of Figure 5b with the solid line of Figure 5a, we see that the Huygens termination underwent the

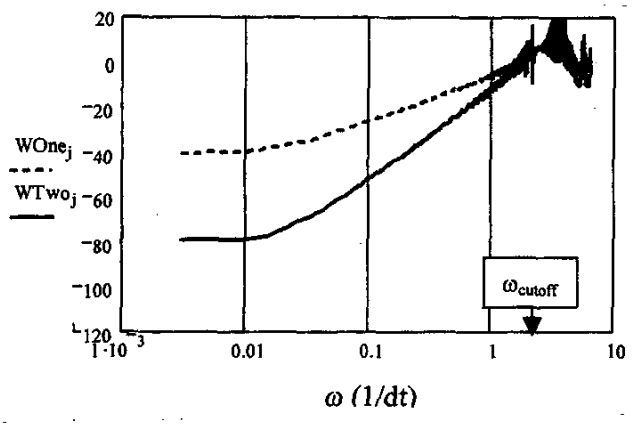

Figure 4b. The attenuation as a function of frequency for one rRBC wall (dashed curve) and for a stack of two walls (solid curve).

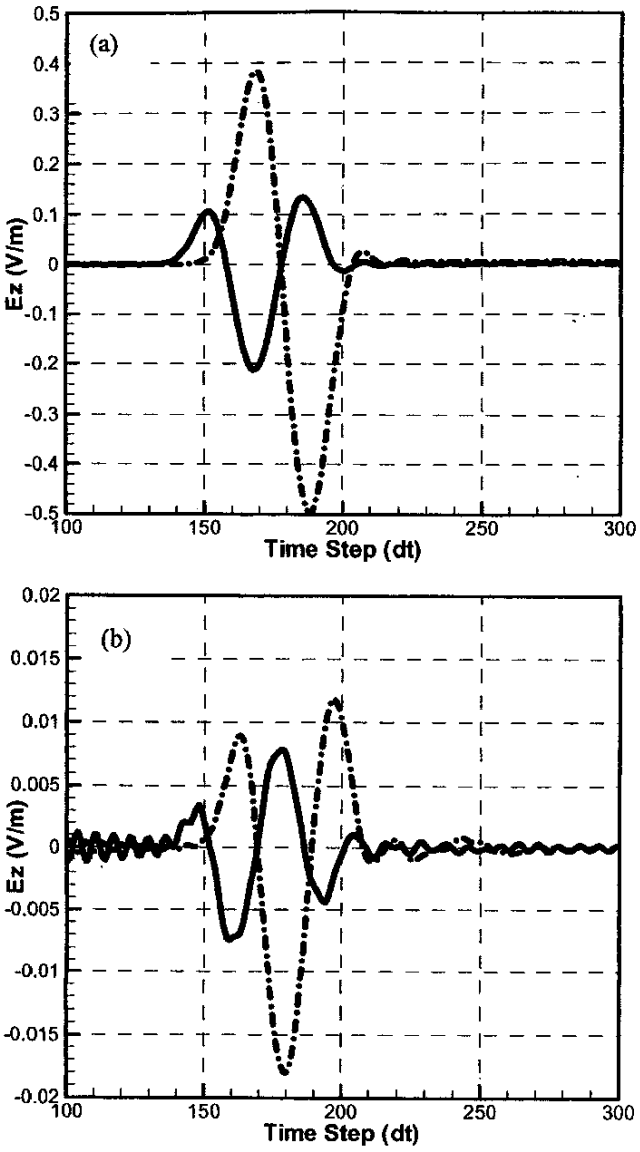

Figure 5. After attenuation going forward through the rRBC (solid line in a), the same pulse gains energy (dashed line in a) if it returns unchanged backwards through the rRBC. Attenuating the pulse by reflection from the Huygens boundary (solid line in b) reduces this energy gain (dashed line in b), making the net echo approximately –37 dB below the input pulse.

integrating effect of going backwards through the RBC, and added another −20 dB of attenuation to the original rRBC.

A two-rRBC stack terminated in a Huygens wall only occupies six cells of the FDTD domain, and provides excellent broadband attenuation. Figure 6 shows that the normal-incidence reflection coefficient varied from −80 dB at low frequencies to −20 dB at the grid cutoff.

Finally, we demonstrated the shallow-angle performance of the rRBC stack. As the inset in Figure 7 shows, a line source was placed in a large two-dimensional space in the presence of a lossy dielectric half-space. The simulation was run first in an oversized domain, and the fields reaching the dashed line were recorded. Then, the domain was truncated at the dashed line with a three-wall rRBC stack. The difference between the fields measured in the presence of the rRBC and those in the oversized space constituted the reflection from the rRBC. This is plotted in Figure 7 as a function of the apparent angle of incidence to the rRBC boundary (ignoring refraction). The results for three frequencies are shown centered around the frequency at which there were 15 cells per wavelength in the dielectric. Note that the reflection coefficient was better than −70 dB for all angles of incidence up to 80°, and then degraded to −40 dB at grazing (90°) in air, and −20 dB at grazing in the dielectric. By comparison, a 10-cell PML used by Yu et al. in a waveguide-simulator test [5] degraded linearly as a function of angle of incidence, from −70 dB at 45° through −50 dB at 60° to 0 dB at grazing.

Two other items should be noted. The wave incident perpendicular to the rRBC is extremely close to the source, and is therefore not a plane wave. This is the reason we saw attenuations of the order of −80 dB to −90 dB near normal instead of the expected −100 dB for a plane wave incident on a three-stack RBC. Second, it should also be noted that there is absolutely no discontinuity in the reflection coefficient upon crossing the dielectric boundary, proving that the rRBC is completely transparent to material properties.

5. Conclusion

A new re-radiating boundary condition for terminating the FDTD grid has been described. Because it is based on the teleportation principle, using exact Schelkunoff currents in FDTD, it works for arbitrary time-varying fields, arbitrary wave impedance (plane waves, spherical waves, near fields), and arbitrary material properties. It is also trivial to program into the conventional FDTD, and it is more angle insensitive than the PML.

6. References

1. M. E. Watts and R. E, Díaz, "Perfect Plane-Wave Injection into a Finite FDTD Domain through Teleportation of Fields," *Electromagnetics*, **23**, 2, February-March 2003, pp. 187-201.

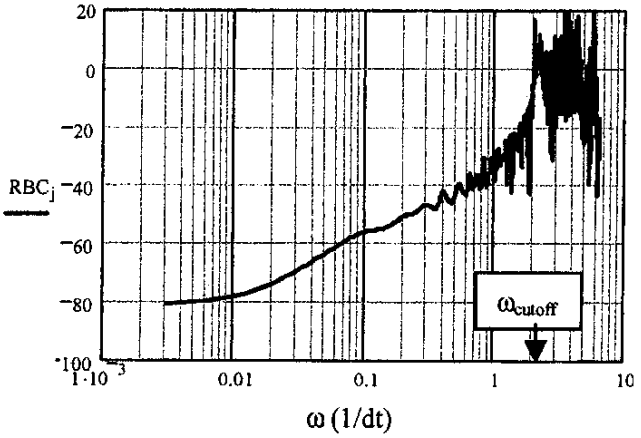

Figure 6. The normal-incidence reflection coefficient for a stack of two rRBCs terminated on a Huygens wall.

2. S. V. Georgakopoulos, C. R. Birtcher, C. A. Balanis, and R. A. Renaut, "Higher-Order Finite-Difference Schemes for Electromagnetic Radiation, Scattering, and Penetration, Part 2: Applications," *IEEE Antennas and Propagation Magazine*, **44**, 2, April 2002, pp. 92-101.

3. J. P. Berenger, "A Perfectly Matched Layer for the Absorption of Electromagnetic Waves," *J. Comp. Phys.*, **114**, 1994, pp. 185-200.

4. S. D. Gedney, "An Anisotropic Perfectly Matched Layer-Absorbing Medium for the Truncation of FDTD Lattices," *IEEE Transactions on Antennas and Propagation*, **AP-44**, December 1996, pp. 1630-1639.

5. W. Yu, R. Mittra, and D. H. Werner, "FDTD Modeling of an Artificially Synthesized Absorbing Medium," *IEEE Microwave and Guided Wave Letters*, **9**, 12, December 1999, pp. 496-498.

2004 USNC/URSI National Radio Science Meeting Student Paper Awards

The winners of the Student Paper Awards were announced at the Plenary Session of the 2004 USNC/URSI National Radio Science Meeting on January 6, 2004, in Boulder, Colorado. First prize ($1000 plus travel expenses) was awarded to Fernanda São Sabbas (Figure 1) for the paper, "Role of Neutral Density and Conductivity Spatial Structures in Determining Sprite Initiation Locations," co-authored by Davis D. Sentman and Antonius Otto (Geophysical Institute of Alaska, Department of Physics, University of Alaska, Fairbanks, Alaska). Second prize ($500 plus travel expenses) was awarded to Nader Behdad (Figure 2) for the paper, "A Novel Quad-Pole Slot Antenna with Very Large Bandwidth," co-authored by Kamal Sarabandi (Department of Electrical Engineering and Computer Science, University of Michigan, Ann Arbor, Michigan). Third prize ($500 plus travel expenses) was awarded to Aycan Erentok (Figure 3) for the paper, "Metamaterial Realizations of Artificial Magnetic Conductors," co-authored by Richard W. Ziolkowski (Department of Electrical and Computer Engineering, University of Arizona, Tucson, Arizona). The Student Paper Contest was chaired by Steven C. Reising.

Figure 1. Fernanda São Sabbas (r) received the First Prize in the 2004 USNC/URSI National Radio Science Meeting Student Paper Contest from Steven Reising.

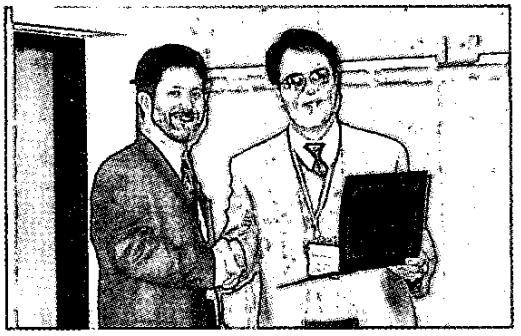

Figure 2. Nader Behdad (r) received the Second Prize.

Figure 3. Aycan Erentok (r) received the Third Prize.

Figure 4. (l-r) Umran Inan, Chair of USNC/URSI; Nader Behdad; Fernanda São Sabbas; Aycan Erentok; and Steven Reising, Chair of the Student Paper Contest.